








Modelling the Dynamics of a Large-Scale Industrial Manipulator for Precision Control

M. P. Cartmell¹  , I. Gordon², D. Johnston¹, S. Liang² , L. McIntosh² ,
and B. Wynne^{1,2} 

¹ Department of Mechanical and Aerospace Engineering, University of Strathclyde, James Weir Building, 75 Montrose Street, Glasgow G1 1XJ, Scotland, UK

matthew.cartmell@strath.ac.uk

² Advanced Forming Research Centre, 85 Inchinnan Drive, Inchinnan, Renfrewshire PA4 9LJ, Scotland, UK

Abstract. *FutureForge* is a strategic programme in the University of Strathclyde Advanced Forming Research Centre (AFRC) to deliver a 2,000 Tonne hydraulic press acting in three forging modes; open die, closed die and isothermal mode. A key element of *FutureForge* relates to the development of a digital environment and simulation capability. The forging environment has been designed, and the principal aim of this research is to develop a nonlinear mathematical model of the manipulator dynamics. The manipulator is used to carry the metal ingots/bars from storage to the furnaces and then feed them to the hydraulic press to undergo the forging operation. This model is required for developing a VR capability which can be used to train operators and engineers who will be required to use the system in practice. It is also forming the basis of a new nonlinear control strategy for the machine.

Keywords: Kinematics · Nonlinear · Constraints · Dynamics · Control · Digital environment

1 Introduction

The manipulator design is based upon three coupled parallelogram linkage sub-systems fitted with two independent hydraulic cylinders that are configured to provide decoupled vertical and horizontal motions of the manipulator end-effector. The modelling is based upon classical Lagrangian mechanics in which the mechanism is split into two separate operational phases which physically share the three parallelogram linkages, operating appropriately to drive the end-effector vertically or horizontally, as required. It is shown that any combination of two-dimensional motion of the end-effector can be achieved, from any starting point to any end point location within the allowable configuration space of the manipulator. The two-dimensional kinematics of the system are described in terms of two generalised angular coordinates referred to an Earth fixed frame of reference, with associated generalised forces that originate physically from the hydraulic cylinders, and the system geometry. It is found that certain kinematic constraints imposed by the design

are required to preserve the uniformity of the parallelogram linkage geometry during all aspects of operation, and that some simplification of the mathematical expression of this aspect of the kinematics is required for efficient computation.

2 Analysis of the Vertical Actuation Phase

From Fig. 1 it can be noted that there are three angles, α , β , γ required to specify fully the position and orientation of the machine. This system has some of the kinematic properties of a parallel robot, requiring careful geometrical analysis [1].

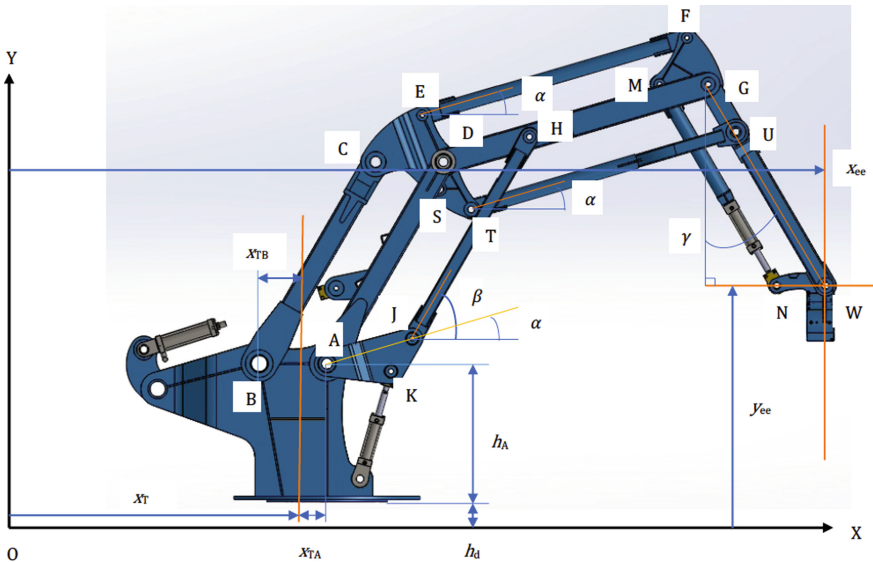


Fig. 1. Schematic side elevation of the *FutureForge* manipulator with reference to an Earth-fixed frame of reference.

As the vertical and horizontal operations have been designed to be completely separate it can be seen that during any vertical motion β and γ are constants and $\alpha = \alpha(t)$, where this is the generalised co-ordinate required to specify the motion of the machine under vertical actuation. On that basis the vertical position of the end-effector is defined by,

$$y_{ee} = h_d + h_A + l_{AJ} \sin \alpha(t) + l_{JH} \sin \beta + l_{HG} \sin \alpha(t) - l_{GW} \cos \gamma \quad (1)$$

and the horizontal position of the end-effector is given by,

$$x_{ee} = x_T + x_{TA} + l_{AJ} \cos \alpha(t) + l_{JH} \cos \beta + l_{HG} \cos \alpha(t) + l_{GW} \sin \gamma \quad (2)$$

So, we can calculate the two-dimensional position of the end-effector, considered here to be at a selectable and arbitrary location on W. By referring to Fig. 1, the linkages

which move during vertical actuations are seen to be: AJK, DG, EF, TU, HJ, FGM, GW, MN, and NW. We now need to evaluate the vertical positions above the OX datum of all these linkages associated with vertical actuations. Link AJK is triangular so the centroid of this link is located at

$$C_{AJK} = \left(\frac{1}{3}(x_A + x_J + x_K), \frac{1}{3}(y_A + y_J + y_K) \right). \tag{3}$$

We can assume direct knowledge of (x_A, y_A) from Fig. 1, so from Fig. 2(a), we see that the relative angular positions of A, J, and K are defined by means of α, η, μ , where $\eta(t) = \mu - \alpha(t)$, leading to,

$$\begin{aligned} x_J &= x_A + l_{AJ} \cos \alpha(t) & x_K &= x_A + l_{AK} \cos \eta(t) \\ y_J &= y_A + l_{AJ} \sin \alpha(t) & y_K &= y_A - l_{AK} \sin \eta(t). \end{aligned} \tag{4}$$

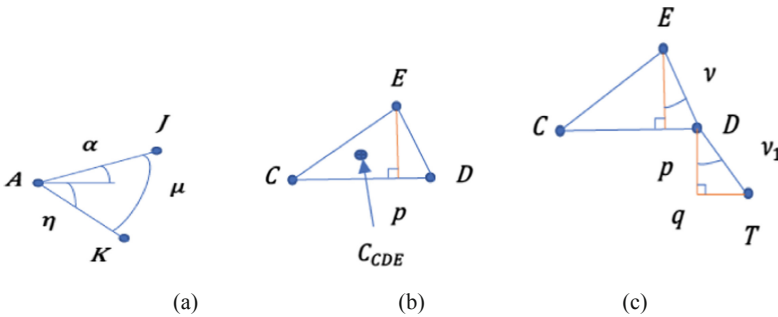


Fig. 2. (a) The relationships between angles α, η, μ on link AJK. The argument t has been dropped from $\alpha(t)$ and $\eta(t)$ for clarity. (b) Location of position p below E , and centroid, on link CDE . (c) Links CDE and DT and angles ν and ν_1 .

Also, we note from Fig. 1 that $x_A = x_T + x_{TA}$ and $y_A = h_A + h_d$, so the absolute two-dimensional location of C_{AJK} (where here ‘absolute’ means with reference to the origin of the Earth-fixed frame OXY) is given by,

$$C_{AJK} = \left(\left(x_T + x_{TA} + \frac{l_{AJ}}{3} \cos \alpha(t) + \frac{l_{AK}}{3} \cos \eta(t) \right), \left(h_A + h_d + \frac{l_{AJ}}{3} \sin \alpha(t) \right) \right), \left(-\frac{l_{AK}}{3} \sin \eta(t) \right) \tag{5}$$

Substituting for $\eta(t)$ gives the centroidal position in terms of $\alpha(t)$ and μ , and we just take the vertical part of this,

$$y_{C_{AJK}} = h_A + h_d + \frac{l_{AJ}}{3} \sin \alpha(t) - \frac{l_{AK}}{3} \sin(\mu - \alpha(t)). \tag{6}$$

Link DG rotates around D and its centroid is at C_{DG} . Link DG orientates through $\alpha(t)$ irrespective of the instantaneous positions of β and γ , confirmed by the animated

CAD. We note also that AD//JH. So, from Fig. 1, we have the following, on the basis that the centroid is located half-way along the length of the link,

$$y_{CDG} = h_A + h_d + l_{AD} \sin \beta + \frac{l_{DG}}{2} \sin \alpha(t). \tag{7}$$

In the case of link EF we see again from Fig. 1 that EF//DG//TU. We also confirmed from the designer’s animated CAD that CD remains horizontal throughout any vertical motion, so,

$$y_D = y_C = h_A + h_d + l_{BC} \sin \beta, \quad x_D = x_C + l_{CD} = x_T - x_{TB} + l_{BC} \cos \beta + l_{CD} \tag{8}$$

In order to deal with point E we consider the geometry of the triangular link CDE, Fig. 2(b), where $E_p \perp CD$, so,

$$x_E = x_C + l_{Cp} = x_T - x_{TB} + l_{BC} \cos \beta + l_{Cp} \tag{9}$$

and from Fig. 2(b) we also get,

$$y_E = h_A + h_d + l_{BC} \sin \beta + l_{Ep}. \tag{10}$$

Now we know the coordinates of E we calculate the height of the centroid (taken half-way along EF) from the OX datum,

$$y_{CEf} = h_A + h_d + l_{BC} \sin \beta + l_{Ep} + \frac{l_{EF}}{2} \sin \alpha(t). \tag{11}$$

Next, we take link TU and we see from the animated CAD that DT remains in a fixed orientation during any vertical motion. Figure 2(c), shows the geometry of links CDE and DT within the kinematically constraining rear-rocker. Proceeding on the basis that $v \simeq v_1$, implied by the animated CAD, then trigonometry leads to, $v = \sin^{-1} \left(\frac{l_{pD}}{l_{ED}} \right) \simeq v_1$. So, as $l_{Dq} = l_{DT} \cos \left(\sin^{-1} \left(\frac{l_{pD}}{l_{ED}} \right) \right)$ then we get the following for the vertical height of T above the OX datum, y_{TT} ,

$$y_{TT} = h_A + h_d + l_{BC} \sin \beta - l_{DT} \cos \left(\sin^{-1} \left(\frac{l_{pD}}{l_{ED}} \right) \right). \tag{12}$$

This is a very minor approximation and has been substantiated by a general observation from the animated CAD that $v \simeq v_1$. Knowing y_{TT} allows us to find the height of the centroid C_{TU} above the OX datum, as follows,

$$y_{CTU} = h_A + h_d + l_{BC} \sin \beta - l_{DT} \cos \left(\sin^{-1} \left(\frac{l_{pD}}{l_{ED}} \right) \right) + \frac{l_{TU}}{2} \sin \alpha(t). \tag{13}$$

From this we move on to link JH and note that as we have dealt with link AJK we already know y_{CAJK} . But we also need y_J to be able to specify y_{CJH} . We can obtain y_J directly from Fig. 1, therefore,

$$y_J = h_A + h_d + l_{AJ} \sin \alpha(t) \tag{14}$$

from which we can write,

$$y_{C_{JH}} = h_A + h_d + l_{AJ} \sin \alpha(t) + \frac{l_{JH}}{2} \sin \beta. \tag{15}$$

Link FGM is another triangular component and the two-dimensional centroidal location is defined by,

$$C_{FGM} = \left(\frac{1}{3}(x_F + x_G + x_M), \frac{1}{3}(y_F + y_G + y_M) \right). \tag{16}$$

We already have y_D and y_E so we can immediately obtain y_G and y_F , respectively, from Fig. 1, as follows,

$$y_G = h_A + h_d + l_{BC} \sin \beta + l_{DG}, y_F = h_A + h_d + l_{BC} \sin \beta + l_{EP} + l_{EF} \sin \alpha(t). \tag{17}$$

Link FGM does not rotate during vertical motion so $MG//OX$ and hence $y_M = y_G$, for all vertical motion cases. So,

$$y_M = h_A + h_d + l_{BC} \sin \beta + l_{DG} \sin \alpha(t). \tag{18}$$

We also need the x-coordinates for points F, G, and M, and these can be calculated from the following. First of all, x_G can be obtained directly from x_{ee} given in Eq. (2), up to joint G, so,

$$x_G = x_T + x_{TA} + l_{AJ} \cos \alpha(t) + l_{JH} \cos \beta + l_{HG} \cos \alpha(t). \tag{19}$$

Given that $MG//OX$ then $x_M = x_G - l_{GM}$,

$$x_M = x_T + x_{TA} + l_{AJ} \cos \alpha(t) + l_{JH} \cos \beta + l_{HG} \cos \alpha(t) - l_{GM} \tag{20}$$

And then, as $x_F = x_E + l_{EF} \cos \alpha(t)$ we get,

$$x_F = x_T - x_{TB} + l_{BC} \cos \beta + l_{Cp} + l_{EF} \cos \alpha(t). \tag{21}$$

Finally, we can put the centroidal y-coordinate together for FGM using Eqs. (17) and (18) to obtain,

$$y_{C_{FGM}} = h_A + h_d + \frac{l_{EP}}{3} + l_{BC} \sin \beta + \frac{l_{EF}}{3} \sin \alpha(t) + \frac{2l_{DG}}{3} \sin \alpha(t). \tag{22}$$

We can also compute the centroidal x-coordinate for FGM, using Eqs. (19)–(21),

$$x_{C_{FGM}} = x_T - \frac{x_{TB}}{3} + \frac{l_{Cp}}{3} + \frac{l_{BC}}{3} \cos \beta + \frac{l_{EF}}{3} \cos \alpha(t) + \frac{2x_{TA}}{3} + \frac{2l_{AJ}}{3} \cos \alpha(t) + \frac{2l_{JH}}{3} \cos \beta + \frac{2l_{HG}}{3} \cos \alpha(t) - \frac{l_{GM}}{3}. \tag{23}$$

Moving on now to link GW. This link moves with a fixed orientation throughout any vertical motion due to the geometry of the parallelogram linkage MGWN, but as

G moves along a circular locus with respect to D then W also moves along this locus. So, we can find (x_W, y_W) by considering the orientation defined by γ . Proceeding from G and using Eqs. (17) and (19) and from Fig. 1, we see that $x_W = x_G + l_{GW} \sin \gamma$ and $y_W = y_G - l_{GW} \cos \gamma$ from which we get,

$$x_W = x_T + x_{TA} + l_{AJ} \cos \alpha(t) + l_{JH} \cos \beta + l_{HG} \cos \alpha(t) + l_{GW} \sin \gamma \quad (24)$$

$$y_W = h_A + h_d + l_{BC} \sin \beta + l_{DG} \sin \alpha(t) - l_{GW} \cos \gamma. \quad (25)$$

It is a simple step from here to find the centroidal coordinates for GW,

$$x_{C_{GW}} = x_T + x_{TA} + l_{AJ} \cos \alpha(t) + l_{JH} \cos \beta + l_{HG} \cos \alpha(t) + \frac{l_{GW}}{2} \sin \gamma \quad (26)$$

$$y_{C_{GW}} = h_A + h_d + l_{BC} \sin \beta + l_{DG} \sin \alpha(t) - \frac{l_{GW}}{2} \cos \gamma. \quad (27)$$

A similar procedure can be undertaken to obtain the coordinates for points M and N, and then the centroidal coordinates for MN. We start from the premise that MG//NW//OX during all vertical motions, so $y_M = y_G$ and $y_N = y_W$. Also, $x_M = x_G - l_{MG}$ and $x_N = x_W - l_{NW}$, so the following constructions emerge,

$$x_M = x_T + x_{TA} + l_{AJ} \cos \alpha(t) + l_{HG} \cos \alpha(t) + l_{JH} \cos \beta - l_{GM} \quad (28)$$

$$x_N = x_T + x_{TA} + l_{AJ} \cos \alpha(t) + l_{HG} \cos \alpha(t) + l_{JH} \cos \beta + l_{GW} \sin \gamma - l_{NW} \quad (29)$$

$$y_M = h_A + h_d + l_{BC} \sin \beta + l_{DG} \sin \alpha(t) \quad (30)$$

$$y_N = h_A + h_d + l_{BC} \sin \beta + l_{DG} \sin \alpha(t) - l_{GW} \cos \gamma. \quad (31)$$

The centroidal coordinates for MN are therefore,

$$x_{C_{MN}} = x_T + x_{TA} + l_{AJ} \cos \alpha(t) + l_{HG} \cos \alpha(t) + l_{JH} \cos \beta - l_{GM} + \frac{l_{MN}}{2} \sin \gamma \quad (32)$$

$$y_{C_{MN}} = h_A + h_d + l_{BC} \sin \beta + l_{DG} \sin \alpha(t) - \frac{l_{MN}}{2} \cos \gamma. \quad (33)$$

The last link to be considered is NW and as we already have calculated y_N and we know that because MG//NW//OX then $y_N = y_W$, so the height of the centroid of NW above OX is therefore $y_{C_{NW}} = y_N = y_W$, which is,

$$y_{C_{NW}} = h_A + h_d + l_{BC} \sin \beta + l_{DG} \sin \alpha(t) - l_{GW} \cos \gamma. \quad (34)$$

The x-coordinate of the centroid of NW is given by $x_W - \frac{l_{NW}}{2}$, hence,

$$x_{C_{NW}} = x_T + x_{TA} + l_{AJ} \cos \alpha(t) + l_{JH} \cos \beta + l_{HG} \cos \alpha(t) + l_{GW} \sin \gamma - \frac{l_{NW}}{2}. \quad (35)$$

We can write down the remaining centroidal x-coordinates, starting with link AJK and returning to Eq. (5) to get,

$$x_{CAJK} = x_T + x_{TA} + \frac{l_{AJ}}{3} \cos \alpha(t) + \frac{l_{AK}}{3} \cos(\mu - \alpha(t)). \tag{36}$$

In the case of link HJ we know x_J from Eqs. (4) so we can refer to Fig. 1, to complete the expression for x_{CHJ} ,

$$x_{CHH} = x_T + x_{TA} + l_{AJ} \cos \alpha(t) + \frac{l_{JH}}{2} \cos \beta. \tag{37}$$

For link EF we get the centroidal x-coordinate by referring to E first from Eq. (9) and then referring to Fig. 1,

$$x_{CEEF} = x_T - x_{TB} + l_{BC} \cos \beta + l_{CP} + \frac{l_{EF}}{2} \cos \alpha(t). \tag{38}$$

In the case of link DG the simplest approach is to take x_A then extend to D and then on to the centroid of DG, therefore,

$$x_{CDGG} = x_T + x_{TA} + l_{AD} \cos \beta + \frac{l_{DG}}{2} \cos \alpha(t). \tag{39}$$

Finally, the rear-rocker configuration in Fig. 2c, provides the basis for an approximation for the x-coordinate of T, building on from x_D again to get x_{CTU} . So, we can write,

$$x_{CTTU} = x_T + x_{TA} + l_{AD} \cos \beta + l_{DT} \sin\left(\sin^{-1}\left(\frac{l_{PD}}{l_{ED}}\right)\right) + \frac{l_{TU}}{2} \cos \alpha(t). \tag{40}$$

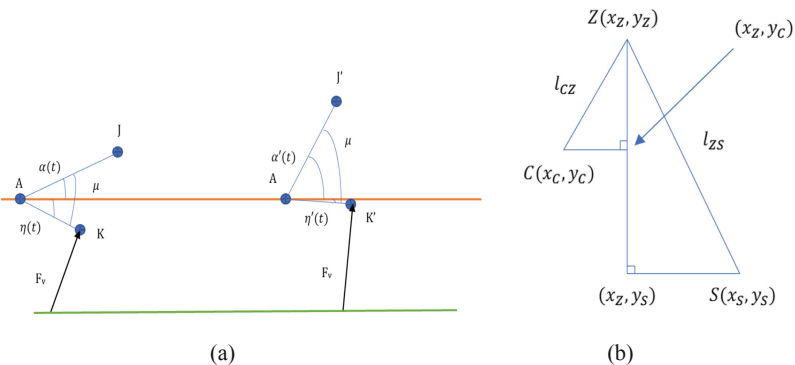


Fig. 3. (a) Virtual work done by force F_v as link AKL rotates through virtual angular displacement $\delta\alpha$. Note that the primes here specifically denote the displaced angular positions. (b) Rear-rocker assembly geometry (coordinates relative to OXY in Fig. 1, and where $x_s > x_z > x_c$ and $y_z > y_c > y_s$).

In order to derive the equations of motion we need the generalised force due to the action of the vertical hydraulic cylinder. The virtual work done by this force as it moves because of a virtual displacement of the generalised co-ordinate is obtained from Fig. 3(a), from which $\alpha(t) + \eta(t) = \mu$ where μ is a constant, so if $\alpha'(t) = \alpha(t) + \delta\alpha(t)$ then $\eta'(t) = \eta(t) - \delta\alpha(t)$ in order to maintain constant μ . The heavy orange line is a grounded horizontal line taken through AB in Fig. 1 and simply extended to the right. The heavy green line is a grounded horizontal line taken through the pin at the bottom end of the cylinder. From this geometry we see that as link AK moves round through $\delta\alpha(t)$, so $\alpha(t) \rightarrow \alpha'(t)$ where $\alpha'(t) = \alpha(t) + \delta\alpha(t)$, then the virtual work done is $\delta W = F_v l_{AK} \delta\alpha(t)$ and so the generalised force is $Q_\alpha = F_v l_{AK}$. This term appears within the equation of motion by applying Lagrange's equation, adding a suitable dissipation term later,

$$\frac{d}{dt} \frac{\partial T}{\partial \dot{\alpha}} - \frac{\partial T}{\partial \alpha} + \frac{\partial U}{\partial \alpha} = Q_\alpha \quad (41)$$

The potential energy is entirely gravitational and the principal masses in the machine for vertical motions are contained in nine components, so from Eqs. 6, 7, 11, 13, 15, 22, 27, 33, 34, the potential energy is,

$$U = (m_{AJK} y_{CAJK} + m_{JHY} y_{CJH} + m_{EFY} y_{CEF} + m_{DGY} y_{CDG} + m_{TUY} y_{CTU} + m_{FGM} y_{CFGM} + m_{MNY} y_{CMN} + m_{GWY} y_{CGW} + m_{NWy} y_{CNW}) g. \quad (42)$$

The kinetic energy terms contain all the two-dimensional translational velocities and also the angular velocities,

$$T = \frac{1}{2} (m_{AJK} \dot{x}_{CAJK}^2 + m_{AJK} \dot{y}_{CAJK}^2 + m_{DYG} \dot{x}_{CDG}^2 + m_{DYG} \dot{y}_{CDG}^2 + m_{EF} \dot{x}_{CEF}^2 + m_{EF} \dot{y}_{CEF}^2 + m_{FGM} \dot{x}_{CFGM}^2 + m_{FGM} \dot{y}_{CFGM}^2 + m_{GW} \dot{x}_{CGW}^2 + m_{GW} \dot{y}_{CGW}^2 + m_{JH} \dot{x}_{CJH}^2 + m_{JH} \dot{y}_{CJH}^2 + m_{MN} \dot{x}_{CMN}^2 + m_{MN} \dot{y}_{CMN}^2 + m_{NW} \dot{x}_{CNW}^2 + m_{NW} \dot{y}_{CNW}^2 + m_{TU} \dot{x}_{CTU}^2 + m_{TU} \dot{y}_{CTU}^2 + I_{AJK} \dot{\alpha}^2 + I_{DG} \dot{\alpha}^2 + I_{EF} \dot{\alpha}^2 + I_{TU} \dot{\alpha}^2). \quad (43)$$

Applying Eq. (41) by using Eqs. (42) and (43) and the generalised force defined above, leads to a nonlinear ordinary differential equation expressed in terms of the generalised coordinate $\alpha(t)$. The Lagrangian derivation, and the formulation of the resulting differential equation were performed symbolically within code written in *Mathematica*TM to guarantee algebraic accuracy. Note that J in Eq. (44) replaces I in Eq. (43) to denote the mass moment of inertia quantities (in order to avoid confusions between I and $\sqrt{-1}$). There is a manually inserted classical linear viscous damping term of the form $C_d \dot{\alpha}(t)$ which operates as an aggregated dissipation term for the viscous joint friction and aerodynamic drag for the machine. Equation of motion (44) is numerically integrated using the *Mathematica*TM package NDSolve [2]. We can calculate the translational responses of virtually any point in the machine, as long as the transformational

kinematics for that part are known in terms of $\alpha(t)$. Eq. (44) is as follows,

$$\begin{aligned}
& \frac{1}{6}(\ddot{\alpha}(t)(l_{EF}m_{FGM}l_{HG}(\frac{4}{3} - \frac{4}{3}\cos(2\alpha(t))) + l_{HG}^2(\frac{4}{3} - \frac{4}{3}\cos(2\alpha(t))) \\
& \left(m_{FGM} + \frac{9}{4}m_{GW} + \frac{9}{4}m_{MN} + \frac{9}{4}m_{NW} \right) + \frac{2}{3}m_{AJK}l_{AK}^2 + 6J_{AJK} + l_{DG}l_{EF}m_{FGM} \\
& \left(\frac{4}{3}\cos(2\alpha(t)) + \frac{4}{3} \right) \\
& + l_{DG}^2(\frac{3}{2}m_{DG} + (\frac{4}{3}\cos(2\alpha(t)) + \frac{4}{3})(m_{FGM} + \frac{9}{4}m_{GW} + \frac{9}{4}m_{MN} + \frac{9}{4}m_{NW})) \\
& + 6J_{DG} + l_{EF}^2(\frac{3}{2}m_{EF} + \frac{2}{3}m_{FGM}) + 6J_{EF} + 6J_{TU} + \frac{3}{2}l_{TU}^2m_{TU} \\
& + l_{AJ}(\ddot{\alpha}(t)(\frac{4}{3}m_{AJK}l_{AK}\cos(\mu) + (\sin(\alpha(t)))^2(\alpha(t))) \\
& (\frac{8}{3}l_{EF}m_{FGM} + l_{HG}(\frac{16}{3}m_{FGM} + 12m_{GW} + 12m_{MN} + 12m_{NW}))) \\
& + g(2m_{AJK} + 6m_{JH})\cos(\alpha(t)) + \dot{\alpha}(t)^2\sin(2\alpha(t)) \\
& (\frac{4}{3}l_{EF}m_{FGM} + l_{HG}(\frac{8}{3}m_{FGM} + 6m_{GW} + 6m_{MN} + 6m_{NW}))) \\
& + l_{AJ}^2(\ddot{\alpha}(t)(\frac{2}{3}m_{AJK} + \cos(2\alpha(t))(-\frac{4}{3}m_{FGM} - 3m_{GW} - 3m_{MN} - 3m_{NW})) \\
& + \frac{4}{3}m_{FGM} + 3m_{GW} + 6m_{JH} + 3m_{MN} + 3m_{NW}) \\
& + \dot{\alpha}(t)^2\sin(2\alpha(t))(\frac{4}{3}m_{FGM} + 3m_{GW} + 3m_{MN} + 3m_{NW})) \\
& + 2g_{AJK}l_{AK}\cos(\mu - \alpha(t)) + 6C_d\dot{\alpha}(t) \\
& - \frac{4}{3}l_{DG}l_{EF}m_{FGM}\dot{\alpha}(t)^2\sin(2\alpha(t)) + 4gl_{DG}m_{FGM}\cos(\alpha(t)) \\
& - \frac{4}{3}l_{DG}^2m_{FGM}\dot{\alpha}(t)^2\sin(2\alpha(t)) + 6gl_{DG}m_{GW}\cos(\alpha(t)) + 6gl_{DG}m_{MN}\cos(\alpha(t)) \\
& + 6gl_{DG}m_{NW}\cos(\alpha(t)) + 3gl_{DG}m_{DG}\cos(\alpha(t)) - 3l_{DG}^2m_{GW}\dot{\alpha}(t)^2\sin(2\alpha(t)) \\
& - 3l_{DG}^2m_{MN}\dot{\alpha}(t)^2\sin(2\alpha(t)) - 3l_{DG}^2m_{NW}\dot{\alpha}(t)^2\sin(2\alpha(t)) + 2gl_{EF}m_{FGM}\cos(\alpha(t)) \\
& + \frac{4}{3}l_{EF}m_{FGM}l_{HG}\dot{\alpha}(t)^2\sin(2\alpha(t)) + 3gl_{EF}m_{EF}\cos(\alpha(t)) \\
& + \frac{4}{3}m_{FGM}l_{HG}^2\dot{\alpha}(t)^2\sin(2\alpha(t)) + 3gl_{TU}m_{TU}\cos(\alpha(t)) + 3m_{GW}l_{HG}^2\dot{\alpha}(t)^2\sin(2\alpha(t)) \\
& + 3l_{HG}^2m_{MN}\dot{\alpha}(t)^2\sin(2\alpha(t)) + 3l_{HG}^2m_{NW}\dot{\alpha}(t)^2\sin(2\alpha(t)) = 6l_{AK}F_v.
\end{aligned} \tag{44}$$

3 Analysis of Horizontal Actuation Defined by 2 Degrees of Freedom

We refer once again to Fig. 1, to analysis the system in detail. In the horizontal scenario the machine traverses left to right or vice versa. Assuming a left to right motion to start with the animated CAD showed that once it reaches the far right position the machine must then either move up or down. The actual choice depends on whether the machine has just traversed in the upper horizontal configuration (UHC), which would have occurred because of a previous vertical lift operation, or the other case where the machine has traversed in the lower horizontal configuration (LHC) which would have occurred because of a previous vertical descent. During UHC and LHC motions the machine is orientated so that α is constant during this phase, and therefore $\alpha \neq \dot{\alpha}(t)$. In the case of UHC we find from the system geometry, available from the animated CAD, that $\alpha = 17.5^\circ$. This is the case for both the left-to-right and right-to-left variants. We initially take the case of UHC left-to-right motion, as this can easily be generalised to all other forms of horizontal motion (noting that $\alpha = -17.5^\circ$ for LHC motions). There

are essentially two angular coordinates associated with the UHC and LHC motions, and these are $\beta(t)$ and $\gamma(t)$. Therefore, Eqs. (1) and (2) now take the following forms,

$$y_{ee} = h_d + h_A + l_{AJ} \sin \alpha + l_{JH} \sin \beta(t) + l_{HG} \sin \alpha - l_{GW} \cos \gamma(t) \quad (45)$$

$$x_{ee} = x_T + x_{TA} + l_{AJ} \cos \alpha + l_{JH} \cos \beta(t) + l_{HG} \cos \alpha + l_{GW} \sin \gamma(t). \quad (46)$$

The kinematic relationships for horizontal motions have partly been established previously, with further ones summarised in the following analysis. We note that the equations that we need for this part of the analysis that have previously been established require the revised generalised co-ordinates for the horizontal motion cases to be implemented. These equations relate to the following links: EF (Eqs. (11) and (38)), DG (Eqs. (7) and (39)), TU (Eqs. (13) and (40)), JH (Eqs. (15) and (37)), MN (Eqs. (32) and (33)), GW (Eqs. (26) and (27)), and FGM (Eqs. (22) and (23)). Starting with link EF,

$$y_{CEF} = h_A + h_d + l_{BC} \sin \beta(t) + l_{Ep} + \frac{l_{EF}}{2} \sin \alpha \quad (47)$$

$$x_{CEF} = x_T - x_{TB} + l_{BC} \cos \beta(t) + l_{Cp} + \frac{l_{EF}}{2} \cos \alpha. \quad (48)$$

Then moving on to link DG,

$$y_{CDG} = h_A + h_d + l_{AD} \sin \beta(t) + \frac{l_{DG}}{2} \sin \alpha \quad (49)$$

$$x_{CDG} = x_T + x_{TA} + l_{AD} \cos \beta(t) + \frac{l_{DG}}{2} \cos \alpha. \quad (50)$$

The next link is TU,

$$y_{CTU} = h_A + h_d + l_{BC} \sin \beta(t) - l_{DT} \cos \left(\sin^{-1} \left(\frac{l_{pD}}{l_{ED}} \right) \right) + \frac{l_{TU}}{2} \sin \alpha \quad (51)$$

$$x_{CTU} = x_T + x_{TA} + l_{AD} \cos \beta(t) + l_{DT} \sin \left(\sin^{-1} \left(\frac{l_{pD}}{l_{ED}} \right) \right) + \frac{l_{TU}}{2} \cos \alpha. \quad (52)$$

Then we consider link JH,

$$y_{CJH} = h_A + h_d + l_{AJ} \sin \alpha + \frac{l_{JH}}{2} \sin \beta(t) \quad (53)$$

$$x_{CJH} = x_T + x_{TA} + l_{AJ} \cos \alpha + \frac{l_{JH}}{2} \cos \beta(t). \quad (54)$$

For link MN we have,

$$y_{CMN} = h_A + h_d + l_{BC} \sin \beta(t) + l_{DG} \sin \alpha - \frac{l_{MN}}{2} \cos \gamma(t) \quad (55)$$

$$x_{CMN} = x_T + x_{TA} + l_{AJ} \cos \alpha + l_{HG} \cos \alpha + l_{JH} \cos \beta(t) - l_{GM} + \frac{l_{MN}}{2} \sin \gamma(t). \quad (56)$$

In the case of link GW the equations are,

$$y_{C_{GW}} = h_A + h_d + l_{BC} \sin \beta(t) + l_{DG} \sin \alpha - \frac{l_{GW}}{2} \cos \gamma(t) \quad (57)$$

$$x_{C_{GW}} = x_T + x_{TA} + l_{AJ} \cos \alpha + l_{JH} \cos \beta(t) + l_{HG} \cos \alpha + \frac{l_{GW}}{2} \sin \gamma(t). \quad (58)$$

Then, we have link FGM for which we apply an identical procedure to that used for link AJK, to locate the centroid,

$$y_{C_{FGM}} = h_A + h_d + \frac{l_{EP}}{3} + l_{BC} \sin \beta(t) + \frac{l_{EF}}{3} \sin \alpha + \frac{2l_{DG}}{3} \sin \alpha \quad (59)$$

$$\begin{aligned} x_{C_{FGM}} = x_T - \frac{x_{TB}}{3} + \frac{l_{CP}}{3} + \frac{l_{BC}}{3} \cos \beta(t) + \frac{l_{EF}}{3} \cos \alpha + \frac{2x_{TA}}{3} + \frac{2l_{AJ}}{3} \cos \alpha \\ + \frac{2l_{JH}}{3} \cos \beta(t) + \frac{2l_{HG}}{3} \cos \alpha - \frac{l_{GM}}{3}. \end{aligned} \quad (60)$$

Finally, we analyse link CDE using one more application of the general procedure for triangular linkages, leading to,

$$x_{C_{CDE}} = x_T - x_{TB} + \frac{l_{CD}}{3} + \frac{l_{CP}}{3} + l_{BC} \cos \beta(t) \quad (61)$$

$$y_{C_{CDE}} = h_A + h_d + \frac{l_{EP}}{3} + l_{BC} \sin \beta(t). \quad (62)$$

Moving to the links that are associated just with horizontal motions, starting with BC. This link rotates about B when the machine undergoes horizontal motions. Therefore,

$$y_{C_{BC}} = h_A + h_d + \frac{l_{BC}}{2} \sin \beta(t) \quad (63)$$

$$x_{C_{BC}} = x_T - x_{TB} + \frac{l_{BC}}{2} \cos \beta(t). \quad (64)$$

The next new link is AD, for which we have,

$$y_{C_{AD}} = h_A + h_d + \frac{l_{AD}}{2} \sin \beta(t) \quad (65)$$

$$x_{C_{AD}} = x_T + x_{TA} + \frac{l_{AD}}{2} \cos \beta(t). \quad (66)$$

Finally, we have to consider link ST, noting that the upper end S (refer to Fig. 1) moves by means of the partially hidden rear-rocker assembly. This assembly is based on the coupled links CZ and ZS, interacting with link ST, as shown in Fig. 3(b). The objective is to obtain results for the centroids defined by $(x_{C_{CZ}}, y_{C_{CZ}})$ and $(x_{C_{ZS}}, y_{C_{ZS}})$. By examining Fig. 3(b) we see that the knowns are l_{CZ} , l_{ZS} , (x_C, y_C) , and (x_S, y_S) , and from that information we can get the unknown position (x_Z, y_Z) , using the following,

$$l_{CZ}^2 = (y_Z - y_C)^2 + (x_Z - x_C)^2 \quad (67)$$

$$l_{ZS}^2 = (y_Z - y_S)^2 + (x_S - x_Z)^2. \quad (68)$$

From this we finally have sufficient information to calculate $(x_{C_{CZ}}, y_{C_{CZ}})$ and $(x_{C_{ZS}}, y_{C_{ZS}})$ respectively, again from the geometries of Fig. 1, and Fig. 3(b),

$$x_{C_{CZ}} = x_T - x_{TB} + l_{BC} \cos \beta(t) + \frac{l_{CZ}}{2} \cos \left(\sin^{-1} \frac{(y_Z - y_C)}{l_{CZ}} \right) \quad (69)$$

$$y_{C_{CZ}} = h_A + h_d + l_{BC} \sin \beta(t) + \frac{l_{CZ}}{2} \sin \left(\sin^{-1} \frac{(y_Z - y_C)}{l_{CZ}} \right) \quad (70)$$

$$x_{C_{ZS}} = x_T + x_{TA} + l_{AD} \cos \beta(t) + l_{DG} \cos \alpha + l_{GU} \sin \gamma(t) - l_{TU} \cos \alpha - l_{ST} \sin \phi(t) - \frac{l_{ZS}}{2} \cos \left(\sin^{-1} \frac{(y_Z - y_S)}{l_{ZS}} \right) \quad (71)$$

$$y_{C_{ZS}} = h_A + h_d + l_{AD} \sin \beta(t) + l_{DG} \sin \alpha - l_{GU} \cos \gamma(t) - l_{TU} \sin \alpha + l_{ST} \cos \phi(t) + \frac{l_{ZS}}{2} \sin \left(\sin^{-1} \frac{(y_Z - y_S)}{l_{ZS}} \right). \quad (72)$$

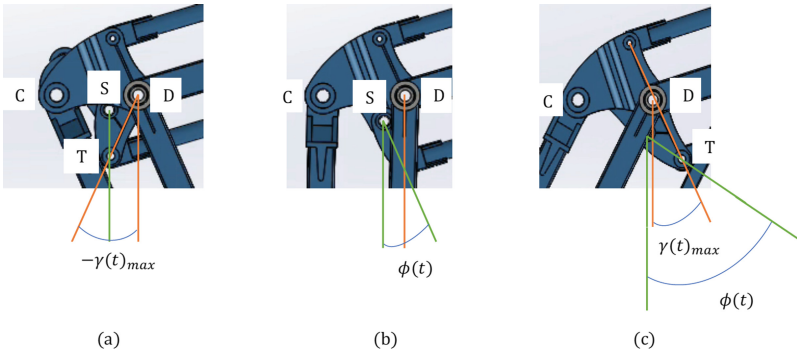


Fig. 4. Local geometry of rear-rocker link ST and the definition of angle $\phi(t)$. (a) $\gamma(t) = -30^\circ$, $\phi(t) = 0$. (b) $\gamma(t) = 0$, $\phi(t) = 30^\circ$. (c) $\gamma(t) = 30^\circ$, $\phi(t) = 60^\circ$.

Where angle $\phi(t)$ is defined between link ST and the local vertical, shown in Fig. 4. The last centroid we require is $(x_{C_{ST}}, y_{C_{ST}})$, and this is represented by,

$$x_{C_{ST}} = x_T + x_{TA} + l_{AD} \cos \beta(t) + l_{DG} \cos \alpha + l_{GU} \sin \gamma(t) - l_{TU} \cos \alpha - \frac{l_{ST}}{2} \sin \phi(t) \quad (73)$$

$$y_{C_{ST}} = h_A + h_d + l_{AD} \sin \beta(t) + l_{DG} \sin \alpha - l_{GU} \cos \gamma(t) - l_{TU} \sin \alpha + \frac{l_{ST}}{2} \cos \phi(t) \quad (74)$$

Analysis of the three principal geometries of Fig. 4, reveals that $\phi(t) = \gamma(t) + 30^\circ$, and this can be substituted into Eqs. (71–74) inclusive. It is straightforward in

principle to evaluate (x_Z, y_Z) analytically but a problem arises in the complexity of the expressions that evolve through the process of solving Eqs. (67) and (68), and even symbolic computation using *Mathematica*TM is impractical as the code rapidly reaches its recursion limit. The solution to this difficulty is to evaluate (x_Z, y_Z) numerically and then to proceed symbolically with the remaining derivation. This overcomes that problem, but we once again find that recursion limits are approached during the full derivation of the differential equations of motion when they include rear-rocker links CZ, ZS, and ST, with the result that computation terminates. Fortunately, the significance of the rear-rocker to the system energies is minimal so its dynamic presence will only emerge strongly through specific resonances, and the machine operates non-resonantly as designed. A numerical evaluation of the mass moments of inertia of the rear-rocker components shows that the rear-rocker contains 1.136% of the overall mass and 0.143% of the total mass moment of inertia of the moving parts of the machine. So the contribution of the rear-rocker to the non-resonant dynamics of the machine is very small, but the rear-rocker is still important because it provides the necessary kinematic constraint for maintaining the upper parallelogram geometry. The generalised force for horizontal cylinder action is obtained from the virtual work done by this force moving through a virtual displacement $\beta(t)$. We see from Fig. 5 that the virtual work done in this case is given by $\delta W = F_H l_{PA} \delta\beta(t)$, and so the generalised force is given by $Q_\beta = F_H l_{PA}$. There is no generalised force associated with the generalised co-ordinate $\gamma(t)$, so $Q_\gamma = 0$.

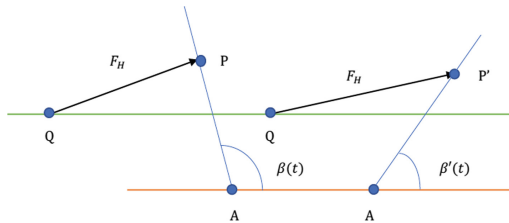


Fig. 5. Virtual work done by force F_H as link length PA rotates through virtual angular displacement $\delta\beta$ where $\delta\beta = \beta(t) - \beta'(t)$. Note that the primes here denote the displaced angular position of link PA .

Now we are able to state the Lagrange equations for the two generalised coordinates defining horizontal motion,

$$\frac{d}{dt} \frac{\partial T}{\partial \dot{\beta}} - \frac{\partial T}{\partial \beta} + \frac{\partial U}{\partial \beta} = Q_\beta = F_H l_{PA}, \tag{75}$$

$$\frac{d}{dt} \frac{\partial T}{\partial \dot{\gamma}} - \frac{\partial T}{\partial \gamma} + \frac{\partial U}{\partial \gamma} = Q_\gamma = 0. \tag{76}$$

From this point onwards the kinetic and potential energies are constructed symbolically and then two nonlinear ordinary differential equations emerge by applying Eqs. (75) and (76). This stage of the derivation has been explored in detail but the two differential equations are unwieldy and long, and numerical solution has not been generally possible. The relationship between $\beta(t)$ and $\gamma(t)$ can be exploited to reduce the horizontal model

down to one generalised co-ordinate. The logical choice is $\beta(t)$ because this is directly actuated by F_H which enters via the generalised force Q_β .

4 Analysis of Horizontal Actuation Defined by 1 Degree of Freedom

Figure 1, shows one of many discrete positions that can be examined for the manipulator in the upper horizontal configuration (UHC) as it moves left-to-right. It can be deduced from these configurations that in general $\gamma(t) = \frac{\pi}{2} - \beta(t)$ (radians) and hence $\dot{\gamma}(t) = -\dot{\beta}(t)$, for both UHC and LHC. The potential energy is given by the following, noting that we require Eqs. (34), (47), (49), (51), (53), (55), (57), (59), (62), (63), (65), (74), where the last equation is modified appropriately so that α is constant and $\beta(t)$ and $\gamma(t)$ are time variant,

$$U = (m_{BC}y_{C_{BC}} + m_{AD}y_{C_{AD}} + m_{CDE}y_{C_{CDE}} + m_{EF}y_{C_{EF}} + m_{DG}y_{C_{DG}} + m_{ST}y_{C_{ST}} + m_{TU}y_{C_{TU}} + m_{JH}y_{C_{JH}} + m_{FGM}y_{C_{FGM}} + m_{MN}y_{C_{MN}} + m_{GW}y_{C_{GW}} + m_{NW}y_{C_{NW}})g. \quad (77)$$

The kinetic energy requires Eqs. (64), (66), (61), (48), (50), (60), (52), (53), (56), (58), (35), (73), (63), (65), (62), (47), (49), (59), (51), (53), (55), (57), (34), and (74), respectively, where Eqs. (34) and (35) are modified appropriately so that α is constant and $\beta(t)$ and $\gamma(t)$ are time variant. Therefore, the kinetic energy is as follows,

$$T = \frac{1}{2}(m_{BC}\dot{x}_{C_{BC}}^2 + m_{BC}\dot{y}_{C_{BC}}^2 + m_{AD}\dot{x}_{C_{AD}}^2 + m_{AD}\dot{y}_{C_{AD}}^2 + m_{CDE}\dot{x}_{C_{CDE}}^2 + m_{CDE}\dot{y}_{C_{CDE}}^2 + m_{EF}\dot{x}_{C_{EF}}^2 + m_{EF}\dot{y}_{C_{EF}}^2 + m_{DG}\dot{x}_{C_{DG}}^2 + m_{DG}\dot{y}_{C_{DG}}^2 + m_{FGM}\dot{x}_{C_{FGM}}^2 + m_{FGM}\dot{y}_{C_{FGM}}^2 + m_{TU}\dot{x}_{C_{TU}}^2 + m_{TU}\dot{y}_{C_{TU}}^2 + m_{JH}\dot{x}_{C_{JH}}^2 + m_{JH}\dot{y}_{C_{JH}}^2 + m_{MN}\dot{x}_{C_{MN}}^2 + m_{MN}\dot{y}_{C_{MN}}^2 + m_{GW}\dot{x}_{C_{GW}}^2 + m_{GW}\dot{y}_{C_{GW}}^2 + m_{NW}\dot{x}_{C_{NW}}^2 + m_{NW}\dot{y}_{C_{NW}}^2 + m_{ST}\dot{x}_{C_{ST}}^2 + m_{ST}\dot{y}_{C_{ST}}^2 + I_{BC}\dot{\beta}^2 + I_{AD}\dot{\beta}^2 + I_{JH}\dot{\beta}^2 + I_{MN}\dot{\gamma}^2 + I_{GW}\dot{\gamma}^2 + I_{ST}\dot{\gamma}^2). \quad (78)$$

We apply Eq. (75) using Eqs. (77) and (78) and the expression for the generalised force Q_β . Then the nonlinear ordinary differential equation in $\beta(t)$ representing all horizontal motions is obtained. Another classical linear viscous damping term is added in the governing equation, of the form $C_d\dot{\beta}(t)$. The equation of motion (79) is strongly nonlinear,

$$\begin{aligned} & -\frac{1}{4}\cos(\beta(t))\sin^2(\alpha)\sin(\beta(t))l_{DG}^2m_{DG}\dot{\beta}(t)^2l_{AD}^2 \\ & +\frac{1}{4}\cos^2(\alpha)\cos(\beta(t))\sin(\beta(t))l_{DG}^2m_{DG}\dot{\beta}(t)^2l_{AD}^2 \\ & +\cos(\beta(t))\sin(\beta(t))m_{TU}\dot{\beta}(t)^2l_{AD}^2 +\frac{1}{4}\cos^2(\beta(t))m_{AD}\dot{\beta}(t)l_{AD}^2 +\frac{1}{4}\sin^2 \\ & (\beta(t))m_{AD}\ddot{\beta}(t)l_{AD}^2 +\frac{1}{4}\cos^2(\beta(t))\sin^2(\alpha)l_{DG}^2m_{DG}\ddot{\beta}(t)l_{AD}^2 +\frac{1}{4}\cos^2(\alpha)\sin^2 \end{aligned}$$

$$\begin{aligned}
& (\beta(t))l_{DG}^2 m_{DG} \ddot{\beta}(t) l_{AD}^2 + \sin^2(\beta(t)) m_{TU} \ddot{\beta}(t) l_{AD}^2 + \frac{1}{2} g \cos(\beta(t)) m_{AD} l_{AD} \\
& + \frac{1}{2} g \cos(\beta(t)) \sin(\alpha) l_{DG} m_{DG} l_{AD} + \cos(\beta(t)) \sin(\beta(t)) l_{BC}^2 m_{EF} \dot{\beta}(t)^2 \\
& - \frac{1}{4} \cos(\beta(t)) \sin^2(\alpha) \sin(\beta(t)) l_{BC}^2 l_{EF}^2 l_{Ep}^2 m_{EF} \dot{\beta}(t)^2 \\
& - \cos(\beta(t)) \sin(\beta(t)) l_{BC}^2 m_{FGM} \dot{\beta}(t)^2 + \frac{1}{4} \cos^2(\alpha) \cos(\beta(t)) \sin(\beta(t)) l_{AJ}^2 l_{JH}^2 m_{JH} \dot{\beta}(t)^2 \\
& - \frac{1}{4} \cos(\beta(t)) \sin(\beta(t)) l_{JH}^2 m_{JH} \dot{\beta}(t)^2 - \cos(\beta(t)) \sin(\beta(t)) l_{BC}^2 m_{TU} \dot{\beta}(t)^2 \\
& + \frac{1}{2} g \cos(\beta(t)) l_{BC} m_{BC} + g \cos(\beta(t)) l_{BC} m_{CDE} + \frac{1}{2} g \cos(\beta(t)) \sin(\alpha) l_{BC} l_{EF} l_{Ep} m_{EF} \\
& + g \cos(\beta(t)) l_{BC} m_{FGM} + g \left(\cos(\beta(t)) l_{BC} - \frac{1}{2} \sin\left(\frac{\pi}{2} - \beta(t)\right) l_{GW} \right) m_{GW} \\
& + \frac{1}{2} g \cos(\beta(t)) l_{JH} m_{JH} + g \left(\cos(\beta(t)) l_{BC} - \frac{1}{2} \sin\left(\frac{\pi}{2} - \beta(t)\right) l_{MN} \right) m_{MN} \\
& + g \left(\cos(\beta(t)) l_{BC} - \sin\left(\frac{\pi}{2} - \beta(t)\right) l_{GW} \right) m_{NW} \\
& + g \left(\cos(\beta(t)) l_{AD} - \sin\left(\frac{\pi}{2} - \beta(t)\right) l_{GU} \right) \\
& + \frac{1}{2} \sin\left(\frac{2\pi}{3} - \beta(t)\right) l_{ST} m_{ST} + g \cos(\beta(t)) l_{BC} m_{TU} + C_d \dot{\beta}(t) + J_{AD} \ddot{\beta}(t) + J_{BC} \ddot{\beta}(t) \\
& + J_{GW} \ddot{\beta}(t) + J_{JH} \ddot{\beta}(t) + J_{MN} \ddot{\beta}(t) + J_{ST} \ddot{\beta}(t) + \frac{1}{4} \cos^2(\beta(t)) l_{BC}^2 m_{BC} \ddot{\beta}(t) \\
& + \frac{1}{4} \sin^2(\beta(t)) l_{BC}^2 m_{BC} \ddot{\beta}(t) + \cos^2(\beta(t)) l_{BC}^2 m_{CDE} \ddot{\beta}(t) + \sin^2(\beta(t)) l_{BC}^2 m_{CDE} \ddot{\beta}(t) \\
& + \sin^2(\beta(t)) l_{BC}^2 m_{EF} \ddot{\beta}(t) + \frac{1}{4} \cos^2(\beta(t)) \sin^2(\alpha) l_{BC}^2 l_{EF}^2 l_{Ep}^2 m_{EF} \ddot{\beta}(t) \\
& + \cos^2(\beta(t)) l_{BC}^2 m_{FGM} \ddot{\beta}(t) + \frac{1}{4} \cos^2(\beta(t)) l_{JH}^2 m_{JH} \ddot{\beta}(t) \\
& + \frac{1}{4} \cos^2(\alpha) \sin^2(\beta(t)) l_{AJ}^2 l_{JH}^2 m_{JH} \ddot{\beta}(t) + \cos^2(\beta(t)) l_{BC}^2 m_{TU} \ddot{\beta}(t) + (\cos(\beta(t)) l_{BC} \\
& - \sin\left(\frac{\pi}{2} - \beta(t)\right) l_{GW}) m_{NW} \left(-\sin(\beta(t)) l_{BC} \dot{\beta}(t)^2 + \cos\left(\frac{\pi}{2} - \beta(t)\right) l_{GW} \dot{\beta}(t)^2 \right. \\
& + \cos(\beta(t)) l_{BC} \ddot{\beta}(t) - \sin\left(\frac{\pi}{2} - \beta(t)\right) l_{GW} \ddot{\beta}(t) \left. + \left(\cos(\beta(t)) l_{BC} - \frac{1}{2} \sin\left(\frac{\pi}{2} \right. \right. \right. \\
& \left. \left. - \beta(t)\right) l_{GW} \right) m_{GW} \left(-\sin(\beta(t)) l_{BC} \dot{\beta}(t)^2 + \frac{1}{2} \cos\left(\frac{\pi}{2} - \beta(t)\right) l_{GW} \dot{\beta}(t)^2 \right. \\
& \left. + \cos(\beta(t)) l_{BC} \ddot{\beta}(t) - \frac{1}{2} \sin\left(\frac{\pi}{2} - \beta(t)\right) l_{GW} \ddot{\beta}(t) \right) \\
& + \left(-\frac{1}{2} \cos\left(\frac{\pi}{2} - \beta(t)\right) l_{GW} - \sin(\beta(t)) l_{JH} \right) m_{GW} \left(-\frac{1}{2} \sin\left(\frac{\pi}{2} - \beta(t)\right) l_{GW} \dot{\beta}(t)^2 \right. \\
& \left. - \cos(\beta(t)) l_{JH} \dot{\beta}(t)^2 - \frac{1}{2} \cos\left(\frac{\pi}{2} - \beta(t)\right) l_{GW} \ddot{\beta}(t) - \sin(\beta(t)) l_{JH} \ddot{\beta}(t) \right)
\end{aligned}$$

$$\begin{aligned}
& + \left(-\frac{1}{3} \sin(\beta(t)) l_{BC} - \frac{2}{3} \sin(\beta(t)) l_{JH} \right) m_{FGM} \left(-\frac{1}{3} \cos(\beta(t)) l_{BC} \dot{\beta}(t)^2 \right. \\
& \left. - \frac{2}{3} \cos(\beta(t)) l_{JH} \dot{\beta}(t)^2 - \frac{1}{3} \sin(\beta(t)) l_{BC} \ddot{\beta}(t) - \frac{2}{3} \sin(\beta(t)) l_{JH} \ddot{\beta}(t) \right) \\
& + \left(-\sin(\beta(t)) l_{JH} - \frac{1}{2} \cos\left(\frac{\pi}{2} - \beta(t)\right) l_{MN} \right) m_{MN} \\
& \left(-\cos(\beta(t)) l_{JH} \dot{\beta}(t)^2 - \frac{1}{2} \sin\left(\frac{\pi}{2} - \beta(t)\right) l_{MN} \dot{\beta}(t)^2 \right. \\
& \left. - \sin(\beta(t)) l_{JH} \ddot{\beta}(t) - \frac{1}{2} \cos\left(\frac{\pi}{2} - \beta(t)\right) l_{MN} \ddot{\beta}(t) \right) + \left(\cos(\beta(t)) l_{BC} - \frac{1}{2} \sin\left(\frac{\pi}{2} \right. \right. \\
& \left. \left. - \beta(t)\right) l_{MN} \right) m_{MN} \left(-\sin(\beta(t)) l_{BC} \dot{\beta}(t)^2 + \frac{1}{2} \cos\left(\frac{\pi}{2} - \beta(t)\right) l_{MN} \dot{\beta}(t)^2 \right. \\
& \left. + \cos(\beta(t)) l_{BC} \ddot{\beta}(t) - \frac{1}{2} \sin\left(\frac{\pi}{2} - \beta(t)\right) l_{MN} \ddot{\beta}(t) \right) + \left(\frac{1}{2} \cos(\alpha) \cos\left(\frac{\pi}{2} \right. \right. \\
& \left. \left. - \beta(t)\right) \cos(\beta(t)) l_{AJ} l_{GW} l_{JH} l_{NW} - \cos(\alpha) \sin(\beta(t)) l_{AJ} l_{JH} \left(\cos(\alpha) l_{HG} - \frac{1}{2} \sin\left(\frac{\pi}{2} \right. \right. \right. \\
& \left. \left. - \beta(t)\right) l_{GW} l_{NW} \right) m_{NW} \left(\frac{1}{2} \cos(\alpha) \cos(\beta(t)) \sin\left(\frac{\pi}{2} - \beta(t)\right) l_{AJ} l_{GW} l_{JH} l_{NW} \dot{\beta}(t)^2 \right. \\
& \left. - \cos(\alpha) \cos\left(\frac{\pi}{2} - \beta(t)\right) \sin(\beta(t)) l_{AJ} l_{GW} l_{JH} l_{NW} \dot{\beta}(t)^2 \right. \\
& \left. - \cos(\alpha) \cos(\beta(t)) l_{AJ} l_{JH} \left(\cos(\alpha) l_{HG} - \frac{1}{2} \sin\left(\frac{\pi}{2} - \beta(t)\right) l_{GW} l_{NW} \right) \dot{\beta}(t)^2 \right. \\
& \left. + \frac{1}{2} \cos(\alpha) \cos\left(\frac{\pi}{2} - \beta(t)\right) \cos(\beta(t)) l_{AJ} l_{GW} l_{JH} l_{NW} \ddot{\beta}(t) \right. \\
& \left. - \cos(\alpha) \sin(\beta(t)) l_{AJ} l_{JH} \left(\cos(\alpha) l_{HG} - \frac{1}{2} \sin\left(\frac{\pi}{2} - \beta(t)\right) l_{GW} l_{NW} \right) \ddot{\beta}(t) \right) \\
& + \left(-\sin(\beta(t)) l_{AD} - \cos\left(\frac{\pi}{2} - \beta(t)\right) l_{GU} + \frac{1}{2} \cos\left(\frac{2\pi}{3} \right. \right. \\
& \left. \left. - \beta(t)\right) l_{ST} \right) m_{ST} \left(-\cos(\beta(t)) l_{AD} \dot{\beta}(t)^2 - \sin\left(\frac{\pi}{2} - \beta(t)\right) l_{GU} \dot{\beta}(t)^2 \right. \\
& \left. + \frac{1}{2} \sin\left(\frac{2\pi}{3} - \beta(t)\right) l_{ST} \dot{\beta}(t)^2 - \sin(\beta(t)) l_{AD} \ddot{\beta}(t) - \cos\left(\frac{\pi}{2} - \beta(t)\right) l_{GU} \ddot{\beta}(t) \right. \\
& \left. + \frac{1}{2} \cos\left(\frac{2\pi}{3} - \beta(t)\right) l_{ST} \ddot{\beta}(t) \right) + \left(\cos(\beta(t)) l_{AD} - \sin\left(\frac{\pi}{2} - \beta(t)\right) l_{GU} \right. \\
& \left. + \frac{1}{2} \sin\left(\frac{2\pi}{3} - \beta(t)\right) l_{ST} \right) m_{ST} \left(-\sin(\beta(t)) l_{AD} \dot{\beta}(t)^2 + \cos\left(\frac{\pi}{2} - \beta(t)\right) l_{GU} \dot{\beta}(t)^2 \right. \\
& \left. - \frac{1}{2} \cos\left(\frac{2\pi}{3} - \beta(t)\right) l_{ST} \dot{\beta}(t)^2 + \cos(\beta(t)) l_{AD} \ddot{\beta}(t) - \sin\left(\frac{\pi}{2} - \beta(t)\right) l_{GU} \ddot{\beta}(t) \right. \\
& \left. + \frac{1}{2} \sin\left(\frac{2\pi}{3} - \beta(t)\right) l_{ST} \ddot{\beta}(t) \right) F_H l_{PA}.
\end{aligned} \tag{79}$$

5 Results

The *FutureForge* manipulator has been modelled in two dimensions as a system of coupled parallelogram linkages which can move under the action of two independent forces to be provided in practice by hydraulic cylinders. The machine can operate independently in its horizontal and vertical modes, so that several different operational sequences can be accommodated. The mathematical modelling works in the same way, separating the motion into horizontal and vertical phases. It has been shown that each phase can be represented by one generalised coordinate, and given the geometrical construction of the machine, and hence its kinematics, the position of any point on the machine within the two-dimensional work-space can be calculated. Therefore, two generalised co-ordinates have been shown to be sufficient to express the full range of operational motions of the machine as a result of forces applied to it, these forces representing the operations of the two hydraulic actuators. The full operation of the machine can be simulated under similar protocols to those on which the designers' animated CAD operates, namely serial vertical and horizontal operations, and vice versa. A practical scenario is initially examined in which the manipulator is initially at the lower left-hand-side so that the machine can execute a left-to-right sweep (this requires the top beam orientation to be -17.5°), and then when the manipulator reaches the end of the sweep at the far right-hand-side (having travelled horizontally for over 5 m) a vertical lift takes place of ~ 2.3 m. This is termed combined motion and is one example of the sort of operation that the machine will undertake in practice. From the computational perspective the two separate models are run sequentially as separate segments of *Mathematica*TM code using the NDSolve package with accuracy controls implemented. The input data and the internal numerical data of the first segment are all cleared before the second segment is evaluated, with the exception of the output results from the first segment (as a parametric plot of the end-effector motion) which are protected and therefore held over. These results are plotted on the same graph as the results from the second segment. The specific solution data for the two phases is given in the caption to Fig. 6. The solver code also contains all the geometrical and mass property data for the machine, extracted at a very high level of accuracy from the CAD. There is not enough room to list this data in full here, but the overall height of the machine when link BC is vertical is 4.992 m, which gives some indication of the size of this machine.

It is interesting to note that there is no discernible vertical lift associated with the horizontal sweep in Fig. 6, at least at the plot scale of the graph, but this is not true for the vertical lift for which there is a noticeable curvature, involving some very obvious horizontal retraction. This occurs because of the kinematics of the design, which imposes circular motion about a fixed centre as a fundamental constituent of the vertical motion of the machine. It is also possible to simulate an imposed oscillation onto the constant forces from either or both hydraulic cylinders, although this obviously has to be of a peak amplitude similar to the static force to generate any noticeable effect in the motion of the end-effector.

Figure 7, defines a horizontal return motion in which the machine travels back from right to left. Figure 7(a), shows the starting orientation from where it begins when going back to the left-hand-side after the combined motions of Fig. 6, and Fig. 7(b), confirms that it is a pure horizontal motion, the difference being that the machine is in the upper

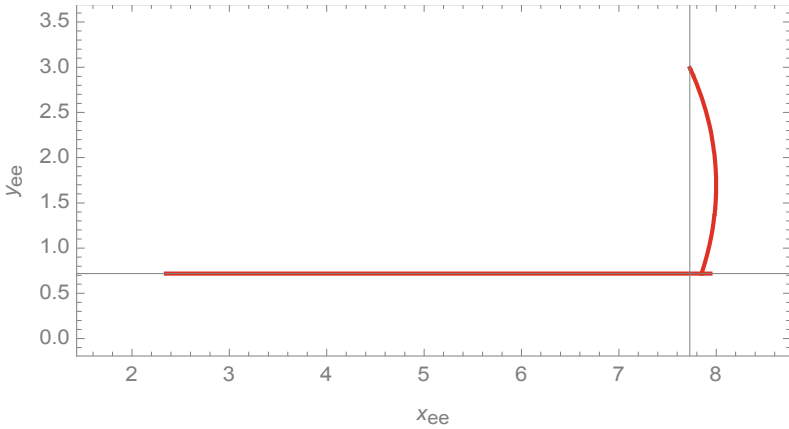


Fig. 6. Combined horizontal and vertical motions plotted in a parametric plot of the motion of the end-effector in time, x_{ee} and y_{ee} plotted in metres. Horizontal: $\alpha = -0.3054$ rad (-17.5°), $F_H = -100$ kN, $C_d = 1000$ Nms, and $t_{end1} = 2.5$ s. $\beta(0) = 2.0944$ rad (120°), $\beta(t_{end1}) = 1.0472$ rad (60°). Vertical: $\beta = 1.0472$ rad (60°), $\mu = 0.3490$ rad (20°), $\gamma = 0.5236$ rad (30°), $F_v = 350$ kN, $C_d = 1000$ Nms, and $t_{ends} = 4.1$ s, $\alpha(t_{end1}) = -0.3054$ rad (-17.5°).

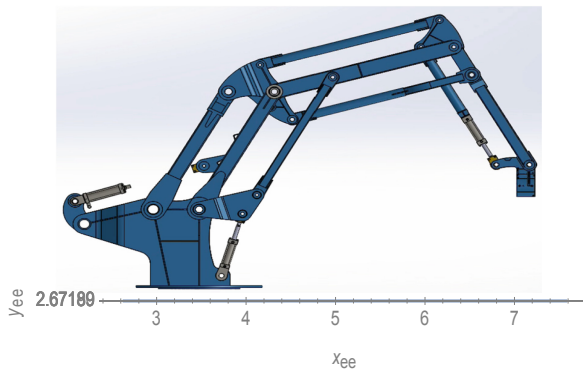


Fig.7. (a) Top, showing starting orientation for horizontal right to left motion, plotted parametrically in (b) below, for: $\alpha = 0.3054$ rad (17.5°). $F_H = 240$ kN, $C_d = 1000$ Nms, and $t_{end} = 1.9$ s, $\beta(0) = 1.1042$ rad (63.2°), $\beta(t_{end}) = 2.0349$ rad (116.6°). x_{ee} and y_{ee} plotted in metres.

horizontal configuration (UHC) for the return sweep. Once again there is no discernible vertical motion when the machine travels horizontally. In fact, this simulation predicts a right-to-left horizontal (UHC) sweep of around 5.0 m, with < 0.01 mm drop.

6 Reduced Order Modelling for Nonlinear Control Implementation

Recent work has focused on trying to reduce the very lengthy differential equations to a compact form, suitable for use in a nonlinear control procedure, as follows:

- Collect like-terms and arranging them into standard forms.

- Evaluate the magnitude (or “significance”) of the constant coefficients of each of these terms as well as their amplitudes and periods (in the case of trigonometric nonlinearities).
- Introduce a small perturbation parameter in accordance with each term’s significance.
- Then determine an appropriate analytical solution procedure, noting that this has been done for the generating problem.

Following this approach, the differential Eqs. (44) and (79) (in $\alpha(t)$, and $\beta(t)$ respectively) can be reduced to the following without loss of generality (removing the time arguments for simplicity),

$$a_1\ddot{\alpha} + a_2\cos(2\alpha)\dot{\alpha} + a_3\dot{\alpha} + a_4\sin(2\alpha)(\dot{\alpha})^2 + a_5\cos(\alpha) + a_6\sin(\alpha) = a_7 \tag{80}$$

$$b_1\ddot{\beta} + b_2\sin(2\beta)\dot{\beta} + b_3\cos(2\beta)\dot{\beta} + b_4\dot{\beta} + b_5\cos(2\beta)(\dot{\beta})^2 + b_6\sin(2\beta)(\dot{\beta})^2 + b_7\cos(\beta) + b_8\sin(\beta) = b_9 \tag{81}$$

The third and fourth terms in Eqs. (80) and (81) respectively are the assumed classical linear viscous damping terms, representing the main mechanisms of joint friction, noting that the aerodynamic damping is vanishingly small in practice. It can be seen that the equations are strongly nonlinear in form. A numerical analysis allows us to see the relative numerical scaling for the first four coefficients of Eq. (80) as an example, as shown in tabulated form below.

Coefficient	Value
a_1	$237.45 + 0.370\cos(\mu)$
a_2	0.0299
a_3	C_d
a_4	0.0299

We see that a_2 and a_4 are both (at least) 100-times smaller than a_1 and a_3 , respectively. Then we introduce a small perturbation parameter, and so insert $a_2 = \varepsilon\bar{a}_2$ and $a_4 = \varepsilon\bar{a}_4$ into the vertical equation of motion, noting that we could even argue numerically that $a_2 = \varepsilon^2\bar{a}_2$ and $a_4 = \varepsilon^2\bar{a}_4$. However, for the time being, we persist with $a_2 = \varepsilon\bar{a}_2$ and $a_4 = \varepsilon\bar{a}_4$. This ordering of terms is consistent with our physical understanding of the system. So, the $\mathcal{O}(\varepsilon^0)$ problem becomes,

$$a_1\ddot{\alpha} + \xi_{joint}\dot{\alpha} + R(\alpha) = a_7 \tag{82}$$

where $R(\alpha)$ is the restoring force. If we plot the potential energy, $E_p = \int R(\alpha)d\alpha$, against the actuation angle, α , then we see the potential is near-linear across the operational range of α .

We can generalise this to get the following for either the vertical or horizontal operations of the actuator, to $\mathcal{O}(\varepsilon^0)$,

$$\ddot{x} + \xi\dot{x} + R(x) = Q \tag{83}$$

and as $\{-\pi/9 \leq \alpha \leq \pi/9\}$, $U_v(\alpha)$ is approximately linear with no stationary points, wells, or turning points. This indicates that the system is non-oscillating to $\mathcal{O}(\varepsilon^0)$. The excitation forces Q can accommodate a suitable static balancing force to counteract the gravitational restoring force within $R(x)$ and then a further time-variant force on top to move the manipulator on a desired trajectory. Note that the work of [3] discusses the possible use of gravity compensators in industrial robots, and that a generalisation of the stiffness modelling approach through the technique of matrix structural analysis is advocated in [4]. This relationship between Q and $R(x)$ applies to both the horizontal and vertical motions. Work continues on expressing the higher order equations correctly, in reduced form, from which the nonlinear dynamics will be examined numerically for all operational modes of motion. A nonlinear control strategy will then be synthesised from that basis.

7 Conclusions

An analytical model of the nonlinear dynamics of a high load capacity manipulator has been derived for the *FutureForge* hydraulic press at the Advanced Forming Research Centre in Inchinnan, Renfrewshire, Scotland, UK. This model is capable of representing any two-dimensional motion that the machine is capable of and this includes the small but important coupling inherent between the vertical and horizontal motions of the end-effector, as seen in Fig. 6. This model is novel in that it preserves the uniformity of perfect parallelogram motion within the three sub-assemblies of the machine, without any restrictions on the configuration space that the manipulator is potentially capable of reaching. This form of modelling could be of interest for other large-scale manipulator designs for these reasons. One could readily imagine actuation scenarios in which the horizontal and vertical phases are interspersed in far more complex ways than shown in Figs. 6 and 7, with specialised trajectories perfectly possible, both physically and mathematically. The equations presented in this paper offer a complete basis for all imaginable trajectories, and therefore further work is required on writing a fully generalised solution code which allows any combinations of motion that might be required in practice. In future the mathematical modelling will be integrated with the 3D animations created by the digital team in AFRC for *FutureForge* simulator training within a visually and kinematically realistic environment, in which the machine works with specific operational trajectories. In parallel with that work a nonlinear control investigation has been started at the University of Strathclyde, based on reduced order modelling, typically as shown in Eqs. (80)–(83) for the initial $\mathcal{O}(\varepsilon^0)$ case. This is work in progress and will be reported on in detail in the future.

Acknowledgements. The authors would like to acknowledge the funding made available through AFRC contract number AFRC_TRP1460_CATP_1466_WP8. They would also like to acknowledge the University of Strathclyde JARA studentship awarded to D.Johnston, with Clansman Dynamics Ltd.

References

1. Cartmell, M.P., Whittaker, A.R., Krimly, A.: The kinematics and dynamics of a dexterous parallel manipulator for structural inspection applications. *Key Eng. Mater.* **293–294**, 653–660 (2005)
2. *Mathematica*TM. <https://www.wolfram.com/mathematica>
3. Xu, P., et al.: Stiffness modeling of an industrial robot with a gravity compensator considering link weights. *Mech. Mach. Theory* **161**, 104331 (2021). <https://doi.org/10.1016/j.mechmachtheory.2021.104331>
4. Klimchik, A., Pashkevich, A., Chablat, D.: Fundamentals of manipulator stiffness modeling using matrix structural analysis. *Mech. Mach. Theory*. **133**, 365–394 (2019). <https://doi.org/10.1016/j.mechmachtheory.2018.11.023>